

SPECIAL COLLECTION: OLIVINE

Accuracy of timescales retrieved from diffusion modeling in olivine: A 3D perspective†

THOMAS SHEA^{1,*}, FIDEL COSTA², DANIEL KRIMER² AND JULIA EVE HAMMER¹

¹Geology and Geophysics, SOEST, University of Hawaii, Honolulu, Hawaii 96822, U.S.A.

²Earth Observatory of Singapore, Nanyang Technological University, 639798, Singapore

ABSTRACT

Diffusion modeling in olivine is a useful tool to resolve the timescales of various magmatic processes. Practical olivine geospeedometry applications employ 1D chemical transects across sections that are randomly sampled from a given 3D crystal population, but the accuracy and precision with which timescales can be retrieved from this procedure are not well constrained. Here, we use numerical 3D diffusion models of Fe-Mg to evaluate and quantify the uncertainties associated with their 1D counterparts. The 3D diffusion models were built using both simple and realistic olivine morphologies, and incorporate diffusion anisotropy as well as different zoning styles. The 3D model crystals were sectioned along ideal or random planes, which were used to perform 1D models and timescale comparisons. Results show that the timescales retrieved from 1D profiles are highly inaccurate and can vary by factors of 0.1–25 if diffusion anisotropy is not taken into account. Even when anisotropy is corrected for, timescales can still vary between 0.2–10 times the true 3D diffusion time due to crystal shape and sectioning effects. Simple grain selection procedures are described to reduce the misfit between calculated and actual diffusion times, and achieve an accuracy and precision of ~5% and ~15–25% relative, respectively. Provided that the grains are carefully selected, about 20 concentration profiles and associated 1D models suffice to achieve this accuracy.

Keywords: Olivine, geospeedometry, diffusion modeling, numerical modeling, crystal morphology, random sectioning

INTRODUCTION

The diffusion of atoms during magmatic reactions (e.g., melting, crystallization, solid-state re-equilibration) can be broadly described as the random jumps or movements of particles relative to other particles in a region of many particles (Onsager 1945; Chakraborty 2008). Because these movements occur at different rates for different chemical components and thermodynamic conditions, modeling of element diffusion can be used for geospeedometry, i.e., to backtrack the durations of geological processes (cf. Watson 1994; Chakraborty 1995, 2008; Ganguly 2002; Watson and Baxter 2007; Costa et al. 2008; Zhang 2010 for reviews). Diffusion modeling is thus becoming an essential utensil of the Earth scientist's toolbox.

This investigation focuses on modeling chemical diffusion in minerals, a technique now regularly used to decipher magma residence times beneath volcanoes (e.g., Zellmer et al. 1999; Costa et al. 2003, 2008; Kahl et al. 2011; Cooper and Kent 2014), magma mixing/recharge events (Morgan et al. 2006; Druitt et al. 2012; Ruprecht and Cooper 2012), ascent times from the mantle (Demouchy et al. 2006; Ruprecht and Plank 2013), and assimilation of crustal material (Bindeman et al. 2006). In particular, olivine is well suited for diffusion studies involving mafic to intermediate magmas, because the diffusion coefficients (D) for

major (Mg, Fe) and minor/trace (Ca, Mn, Cr, Co, Ni) elements are well constrained with respect to temperature (T), forsterite component (X_{Fo}), crystallographic orientation, and oxygen fugacity (f_{O_2}) (e.g., Chakraborty 1997, 2010; Petry et al. 2004; Coogan et al. 2005; Dohmen and Chakraborty 2007; Spandler and O'Neill 2010). As a result, several studies have used diffusion modeling within olivine to decipher the durations associated with various magmatic processes (Nakamura 1995; Coombs et al. 2000; Pan and Batiza 2002; Costa and Chakraborty 2004; Costa and Dungan 2005; Ito and Ganguly 2006; Kahl et al. 2011, 2013; Martí et al. 2013; Ruprecht and Plank 2013; Longpre et al. 2014), and user-friendly diffusion modeling algorithms are becoming available (e.g., DIPRA, Girona and Costa 2013). To date, however, diffusion modeling has been applied to natural magmatic crystals using almost exclusively one-dimensional chemical profiles. Analyses are typically performed along crystals exposed within two-dimensional thin sections, meaning that there are several potential sources of uncertainty: (1) diffusion occurs along the three spatial dimensions of a complex volume (e.g., Costa et al. 2003, 2008); (2) diffusion may occur anisotropically within the mineral, implying that a 1D profile may sample the crystal along a fast or slow direction, or anywhere in between (e.g., Chakraborty 1997); and (3) thin sections intersect crystals randomly, meaning that concentration gradient geometry may be dependent on section orientation and distance from the crystal core (Pearce 1984; Wallace and Bergantz 2004).

In their investigation of Mg in plagioclase, Costa et al. (2003) found that adding a second dimension resulted in shorter calculated

* E-mail: tshea@hawaii.edu

† Special collection papers can be found on GSW at <http://ammin.geoscienceworld.org/site/misc/specialissuelist.xhtml>.

diffusion timescales (i.e., in their case, magma residence times) compared to 1D models. It was also noted that the 1D-derived times were sensitive to the position of the profile with respect to the center of the crystal. The effects of diffusion anisotropy in olivine were also studied in 2D by Costa and Chakraborty (2004), who determined that sections cutting the crystal close to the fast diffusion direction were under certain circumstances more reliable for the retrieval of diffusion timescales. Pan and Batiza (2002) briefly examined the sectioning effect by numerically slicing a sphere containing an artificial diffusion profile, and showed that the recovered timescales followed an exponential distribution, with a low occurrence of durations shorter than the real input time, and a much higher incidence of durations close to the real time.

In this contribution, three-dimensional numerical diffusion models are developed to explore the influence of spatial dimensions, crystal morphology, diffusion anisotropy, and sectioning on the timescales recovered. After examining cases with simple geometries, we allow models to progressively incorporate more complexity. The primary objective is to answer the simple question: how reliable are diffusion timescales retrieved from olivine

crystals as measured in typical thin sections? The importance of this inquiry is illustrated by constructing a numerical thin section containing 200 identical normally zoned olivine crystals that have been randomly sectioned after diffusing for a certain time (Fig. 1). Despite being constructed from the same crystal template, the virtual thin section displays olivine slices that vary significantly in sizes, habits, and apparent concentration gradients. Thus, the diffusion times modeled from 1D profiles sampled within different olivines from this thin section may also differ. In this study, we examine the potential sources of variability in timescales retrieved from 1D diffusion models, and provide olivine crystal selection guidelines to maximize the accuracy and precision. Because parameters affecting timescales are numerous and complexly intertwined, a large number of methods, results, and interpretations sections are provided as Supplementary Material¹ to keep this contribution focused on the essential.

¹ Deposit item AM-15-105163, Supplemental Material and Figures. Deposit items are free to all readers and found on the MSA web site, via the specific issue's Table of Contents (go to <http://www.minsocam.org/MSA/AmMin/TOC/>).

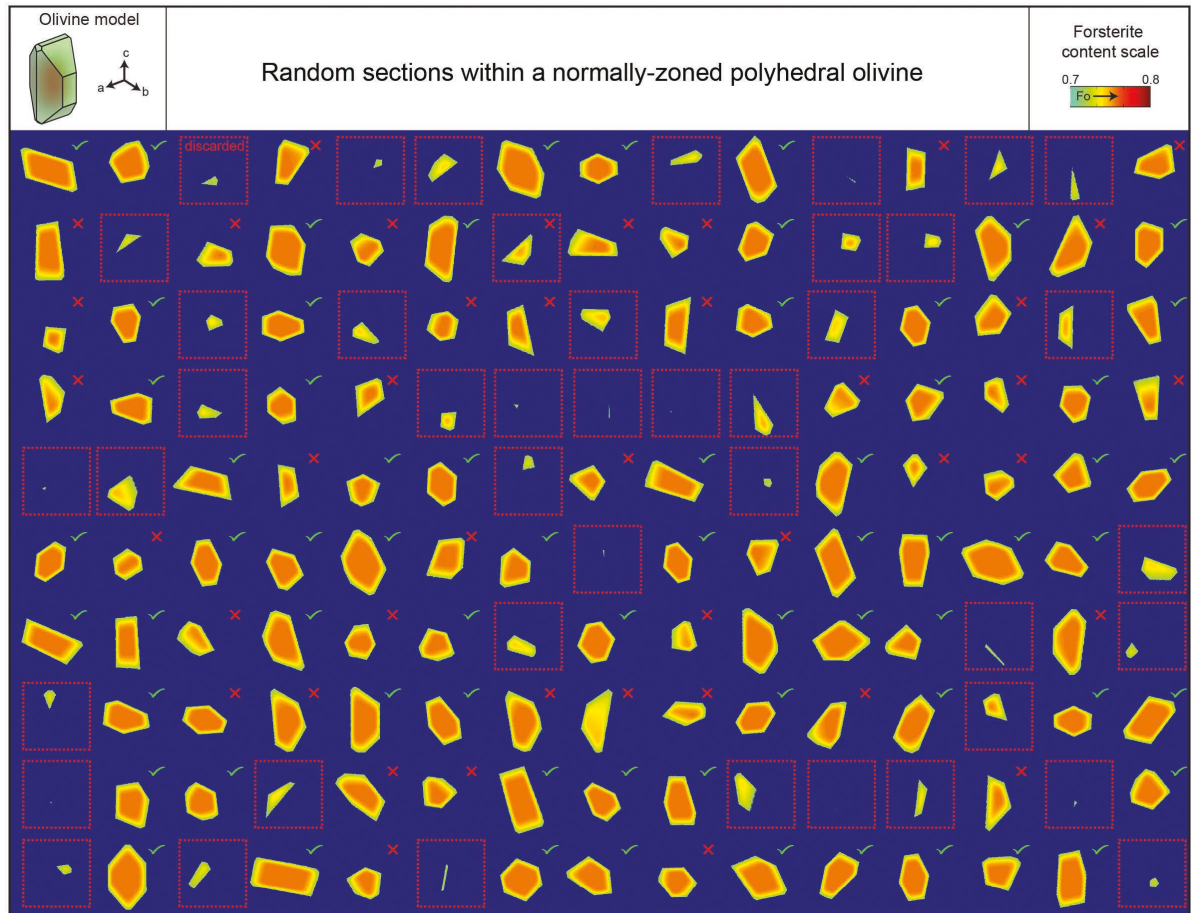


FIGURE 1. Two-dimensional olivine sections within a “virtual” thin section composed of normally zoned crystals sliced randomly from the olivine crystal (top-left panel with a , b , and c being the crystallographic axes). The top-right insert displays the color scale and the equivalent forsterite content. The blue background represents the surrounding glass/melt with which the olivines were equilibrating. The sections outlined by red squares were discarded from further analysis due to their size. The rest were used for timescale comparisons. The green check marks and crosses designate the suitable and unsuitable sections for the purpose of 1D diffusion modeling (see Discussion).

METHOD

This section describes the 1D and 3D models used to simulate diffusion in olivine. After detailing the governing equations and the choice of diffusing components, the numerical implementation and the parameters investigated are described.

Diffusion equation

According to Fick's second law, and if the diffusion coefficient D depends on the composition C of an element i in olivine (see below), the time-dependent 3D diffusion equation (with spatial dimensions x , y , and z , and time t) takes the form (Crank 1975):

$$\frac{\partial C_i}{\partial t} = \left[\frac{\partial}{\partial x} \left(D_x \frac{\partial C_i}{\partial x} \right) + \frac{\partial}{\partial y} \left(D_y \frac{\partial C_i}{\partial y} \right) + \frac{\partial}{\partial z} \left(D_z \frac{\partial C_i}{\partial z} \right) \right] \quad (1)$$

If diffusion is isotropic, a single diffusion coefficient $D_x = D_y = D_z$ suffices to define element mobility within the whole volume. In contrast, if diffusion is anisotropic, and for a crystal belonging to the orthorhombic system with crystallographic axes a , b , and c , the diffusivity tensor takes the form (e.g., Zhang 2010):

$$D = \begin{bmatrix} D_a & 0 & 0 \\ 0 & D_b & 0 \\ 0 & 0 & D_c \end{bmatrix} \quad (2)$$

For the 3D expression given by Equation 1, the diffusivities are therefore defined as $D_x = D_a$, $D_y = D_b$, $D_z = D_c$. The 1D equivalent is simply obtained by removing the y and z components, and replacing D_i by D_a , D_b , D_c , or by an intermediate diffusivity term (e.g., anisotropy-corrected D^* , see below).

Choice of elements and diffusion coefficients

The models in this contribution focus on Fe-Mg in olivine, treated here as the mole fraction of forsteritic component

$$Fo = \frac{Mg}{Mg + Fe}$$

with ($Fo + Fa = 1$, with Fa the fraction fayalite). These elements are commonly used for diffusion modeling (Nakamura 1995; Costa and Chakraborty 2004; Costa and Dungan 2005; Kahl et al. 2011, 2013; Ruprecht and Plank 2013; Longpre et al. 2014), and easy to measure with an electron microprobe. The diffusion coefficient D^{Fe-Mg} is well established for various P , T , f_{O_2} conditions (cf. Chakraborty 2010 and references therein) and known to be strongly anisotropic ($D_a^{Fe-Mg} = D_c^{Fe-Mg} - 1/6 D_b^{Fe-Mg}$; Chakraborty 1997). Along the c axis, the diffusion coefficient D_c^{Fe-Mg} ($m^2 s^{-1}$) is expressed as (Dohmen et al. 2007; Costa et al. 2008; Chakraborty 2010):

$$D_c^{Fe-Mg} = 10^{-9.21} \left(\frac{f_{O_2}}{10^{-7}} \right)^{\frac{1}{6}} 10^{3(0.9 - X_{Fo})} \exp \left(- \frac{201,000 + (P - 10^5) \cdot 7 \times 10^{-6}}{RT} \right) \quad (3)$$

where f_{O_2} is the oxygen fugacity (Pa), X_{Fo} the fraction forsterite, P the pressure (Pa), T the temperature (K), and R the gas constant [$J/(K \text{ mol})$]. In practice, concentration profiles taken across crystal sections are rarely aligned with the main diffusion directions and crystal axes, and must be corrected for orientation as well as anisotropy. Assuming a traverse is measured parallel to the concentration gradient, an anisotropy-corrected diffusivity D^* can be calculated providing that the angles α , β , and γ between the Cartesian coordinates x , y , and z and the crystallographic axes a , b , and c , respectively, are known (Costa and Chakraborty 2004):

$$D^* = D_a \cos^2 \alpha + D_b \cos^2 \beta + D_c \cos^2 \gamma \quad (4)$$

If, instead, the traverse is oblique to the concentration gradient, a more general form of Equation 4 is applicable (Zhang 2010) (cf. Supplementary Material¹), but requires knowledge of the concentration gradient geometry along x , y , and z , which is not accessible within typical 2D thin sections. Because the purpose of this paper is to examine real case scenarios, the simpler form of the anisotropy correction is used herein.

Numerical implementation

The diffusion simulations were performed using finite-differences (e.g., Costa et al. 2003; Kahl et al. 2011; Druitt et al. 2012; Girona and Costa 2013; Pilbeam et al. 2013) (see Supplementary Material¹). For all models, atmospheric pressure conditions ($P = 10^5$ Pa), an oxygen fugacity $f_{O_2} = 3 \times 10^{-12}$ Pa, and a constant temperature $T = 1200$ °C were used. The simulated duration for most experiments was 6 days (144 h), although a few runs with shorter (12 and 72 h) and longer (576 and 864 h) durations were also done. The longer duration was chosen to allow sufficient time for the crystal core compositions to be affected. Olivine crystals with different shapes (see below) were built within a “melt” volume of 241 voxels/side (or 482 μm , with a step size of 2 μm per voxel), allowing for reasonable computation times in 3D runs. The boundaries between crystal and melt were considered open, the melt effectively being an infinite reservoir of Fe-Mg and constant with time. The boundary compositions at the crystal rim were therefore constantly maintained during the runs (e.g., Costa and Chakraborty 2004).

Variables incorporated in the model

The main variables that determine how accurate timescales obtained via diffusion modeling include: (1) the number of spatial dimensions; (2) the anisotropy of diffusion; (3) the shape/morphology of the crystal; (4) the location of the section or profile (i.e., along or off-crystallographic axis, on- or off-center); and (5) the nature of chemical zoning.

The influence of a given variable is difficult to completely isolate from the others, so we decided to organize the diffusion models as follows: First, a series of models tested the influence of crystal shape on retrieved timescales. 1D diffusion models on principal sections along the crystallographic axes were followed by more realistic scenarios that incorporated the effects of section orientation and off-center sectioning. Finally, a representative morphology was selected to explore the effect of variable zoning configurations (normal, reverse, core-rim).

Spatial dimensions. We focused chiefly on comparisons between 1D vs. 3D diffusion, but a few 2D models were also carried out for comparison, and are reported in the Supplementary Material¹.

Crystal shape. Three crystal shapes were examined (Fig. 2a): a sphere with a 201 voxel diameter, a rectangular parallelepiped (hereafter labeled the “orthorhombic” morphology) with dimensions $95 \times 121 \times 201$ voxels (along x , y , and z , corresponding to crystallographic axes a , b , and c), and a realistic olivine morphology (labeled “polyhedral” throughout the text) based on Welsch et al. (2013) with an aspect ratio identical to that of the orthorhomb.

Diffusion anisotropy. For the spherical crystal models we used an isotropic D , while for the orthorhombic crystals we used either isotropic or anisotropic diffusion to evaluate this effect on timescales. The polyhedral crystals were all modeled using anisotropic diffusion (Fig. 2b). The 1D simulations incorporated either a single diffusion coefficient D_a , D_b , D_c (along the axes), or the orientation-corrected coefficient D^* (Eq. 4).

Types of section. The 3D crystal models were sectioned according to four types of planes (Fig. 2c): (1) principal sections (passing through the center, parallel to $a-b$, $b-c$, or $a-c$ planes), hereafter termed “along-axes, on-center” sections, (2) sections parallel to the crystal axes at random distances from the center, so-called “along-axes, off-center,” (3) sections at random angles from the crystallographic axes passing through the center, or “randomly oriented, on-center” and (4) sections at random angles from the axes and distances from the center “randomly oriented, off-center.”

Style of Fo zoning. Six types of compositional zonings were used to simulate a range of magmatic scenarios (Fig. 2d): (1) “normal zoning I,” wherein a crystal of homogeneous composition $C_{ol} = Fo_{90}$ is placed in contact with a melt with an “effective” composition $C_{melt} = Fo_{70}$ (i.e., the equilibrium olivine composition toward which the crystal evolves), (2) “normal zoning II” with a homogenous crystal $C_{ol} = Fo_{75}$ in contact with a similar melt $C_{melt} = Fo_{70}$; these zoning types 1 and 2 mimic the removal of olivine crystals from a mafic melt, and their incorporation into more evolved magmas without rim growth (e.g., magma recharge, Costa and Chakraborty 2004; Kahl et al. 2011). (3) “reverse zoning” with an olivine $C_{ol} = Fo_{70}$ and a melt $C_{melt} = Fo_{80}$; this configuration could represent olivines from the more evolved magma being incorporated into the mafic recharge magma; (4) core-rim I configuration with a core $C_{ol-core} = Fo_{70}$ and a rim $C_{ol-rim} = Fo_{80}$ in contact with a melt $C_{melt} = Fo_{80}$; this type of zoning could also represent a magma mixing event but the olivine has grown a rim prior to diffusive equilibration of the core and the surrounding melt; (5) core-rim II zoning with a core $C_{ol-core} = Fo_{75}$, a rim $C_{ol-rim} = Fo_{70}$ in contact with a melt $C_{melt} = Fo_{80}$; and (6) core-rim III zoning with $C_{ol-core} = Fo_{70}$, $C_{ol-rim} = Fo_{80}$, and $C_{melt} = Fo_{75}$. The last two zoning patterns model more

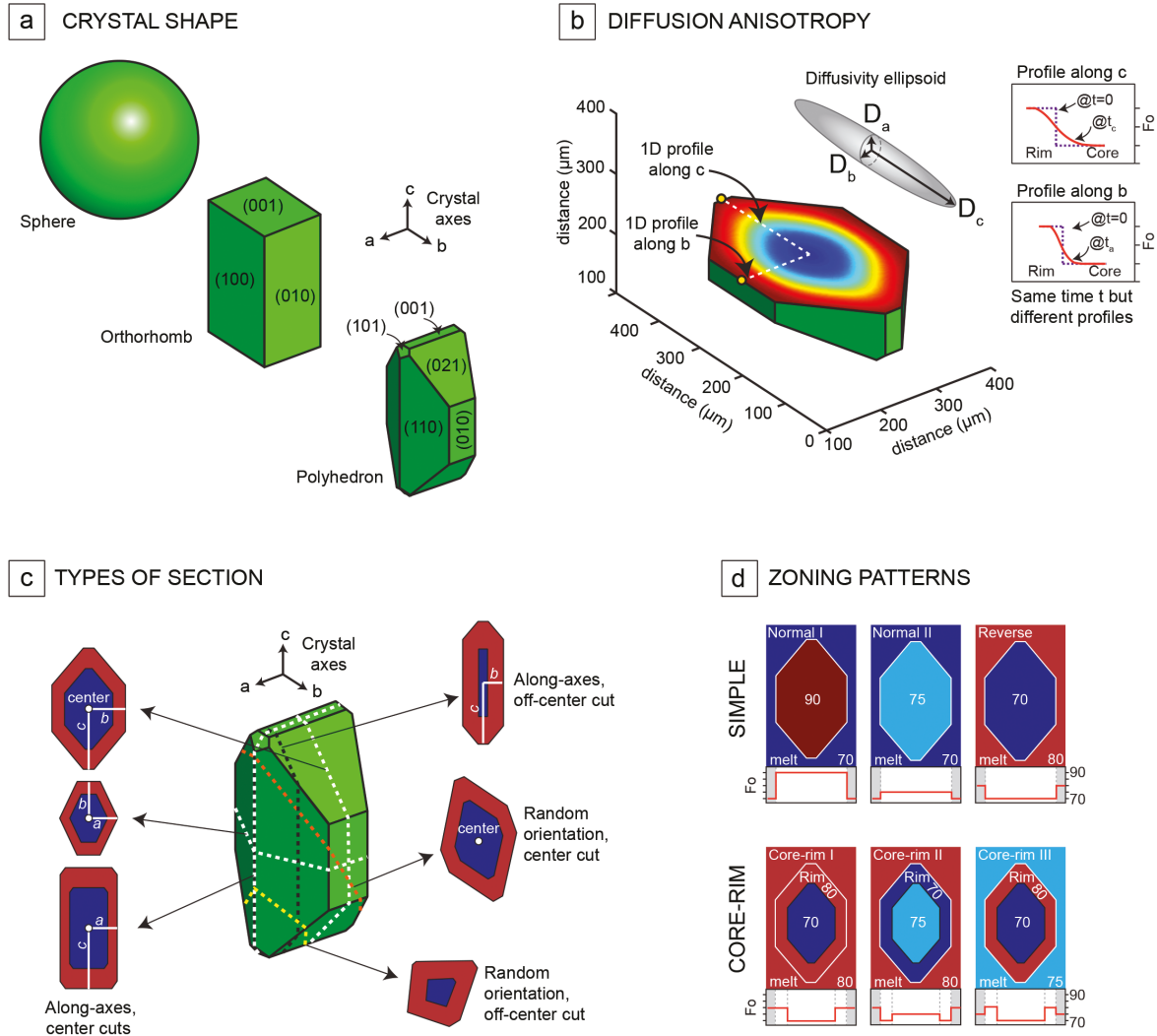


FIGURE 2. Principal variables examined by the diffusion models. (a) The three different crystal shapes tested: a sphere, an orthorhomb, and a polyhedron with the same aspect ratio as the orthorhomb. (b) Anisotropy of Fe-Mg diffusion along the different crystallographic axes (shown as a “diffusivity ellipsoid” in gray). For the same diffusion time t , profiles sampled along different directions in a section appear different. Diffusion modeling of such profiles in 1D may yield different timescales (t_a and t_c along a and c , respectively) if anisotropy is not accounted for (small inserts on the right). (c) Different types of sections considered; principal sections (along-axes, center-cut), sections sampled away from the core and parallel to the axes (along-axes, off-center), sections passing through the core along any orientation (random orientation, center-cut), and randomly oriented sections taken at random distances from the core (random orientation, off-center). (d) Six distinct zoning patterns were evaluated, illustrated here through the b - c plane of the crystal. The corresponding starting Fo concentration profiles are shown below each zoning style. Note that the melt Fo content is displayed as an equivalent olivine Fo composition (i.e., the composition the crystal edge is in equilibrium with).

complex magma interactions in which the growth rim has a different equilibrium Fo composition from that of the surrounding melt. Note that in all simulations, it is assumed that any crystal growth has progressed to completion before diffusion starts (i.e., instantaneous growth with a fixed liquid-crystal boundary).

Procedure for model comparisons

The numerical models were examined according to a systematic protocol, in which 3D simulations were used as ground-truth for comparisons with their 1D counterparts (Fig. 3). This procedure entailed: (1) sectioning the initial 3D olivine crystal before diffusion started; (2) discarding the smallest unsuitable 2D sections when necessary (i.e., for model series involving random sectioning); (3) choosing the suitable section(s) to carry out 1D diffusion models; (4) performing the 3D diffusion simulation; (5) sectioning the 3D “diffused” olivine along the same plane(s) or transect(s) as in steps 1 and 3; and (6) retrieving the 1D timescales that

best match the concentration maps/profiles from the 3D model. The best-fit 1D calculated times are labeled t_{1D}^* , and the true 3D diffusion times t_{3D} (i.e., best-fit times are marked by asterisks). Values of t_{1D}^* were calculated via the root-mean square deviation (RMSD) between the 3D (“real”) and 1D (“measured”) concentration profiles (e.g., Girona and Costa 2013) (see Supplementary Material¹). For a set of parameters, typically one 3D model was used as ground-truth to compare with 200 1D diffusion models. From a set of several hundred sections across the 3D olivine, those that were too small (i.e., typically $<20\%$ in area of the maximum section size observed) were discarded, and the first 100 sections from the leftover set were kept for further analysis (cf. Fig. 1 for an example). For each of these 100 sections, two profiles were manually selected across different crystal faces. To mimic real world practices, 1D transects were always chosen parallel to the concentration gradient within each section. Note that this does not imply, however, that the profiles were parallel to the concentration gradient in the third dimension.

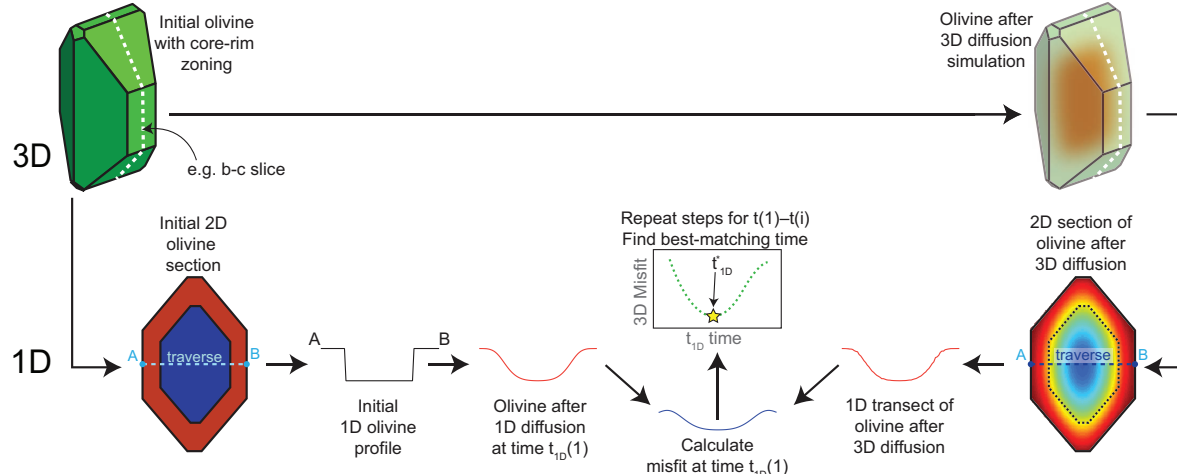


FIGURE 3. Model comparison procedure. A 3D voxelized olivine with a given initial Fo zoning pattern (cf. Fig. 2d) is “cut” prior to diffusion, producing a starting Fo section used to perform 1D diffusion simulations (A–B traverse). The initial 3D olivine diffuses for a certain time, and is sectioned along the same orientation as before to serve as a “ground-truth” for comparison with the 1D model. As the 1D simulations are run, each time step $t(1)$ to $t(i)$ is saved and compared with the ground-truth concentration profile from the 3D model. A minimum misfit is then calculated to yield the best-matching time t_{ID}^* . Also see text for details.

RESULTS AND INTERPRETATIONS

For simplicity, and considering the large number of variables incorporated in the various models (crystal morphology, number of model dimensions, diffusion anisotropy, section orientation, section distance from the core, zoning configuration), results and interpretations are presented one after the other. The following paragraphs first explore the role of crystal morphology and diffusion anisotropy, and later the zoning style. In each case the results are presented in order of increasing sectioning complexity, typically: (1) along-axes, on-center; (2) along-axes off-center; (3) randomly oriented, on-center; and (4) randomly oriented, off-center. Timescales are reported both as absolute values (in hours) and as relative mismatch, defined as

$$r_i(\%) = 100 \times \frac{t_{ID}^* - t_{3D}}{t_{3D}}.$$

In the latter case, zero implies a perfect match, a positive number indicates a time overestimate, and a negative number an underestimate.

Influence of crystal shape and diffusion anisotropy

Two scenarios were tested, with isotropic (for the spherical and orthorhombic crystals) and anisotropic diffusion (for the orthorhombic and polyhedral crystals). For each situation, two 3D models with diffusion times of 72 and 144 h were performed, and the results compared with 1D models. These models were all reversely zoned, with an initially homogenous Fo₇₀ crystal equilibrating with a more mafic melt (Fo₈₀).

Along-axis, on-center sections. For spherical crystals and isotropic D , the best matching 1D time always overestimated the true diffusion time, with $t_{ID}^* = 80$ and 180 h (+10 and +25% the true times $t_{3D} = 72$ and 144 h, respectively) (Figs. 4a and 4b; also see Supplementary Material section 4[†] for corresponding concen-

tration profiles). Models with orthorhombic crystals reproduced the true diffusion times correctly, except for the 144 h models run using isotropic D , which result in slight time overestimates along b and c ($t_{ID}^* \sim 154$ h) (Fig. 4b). The polyhedral morphology yielded 1D times that are either similar to the true times (e.g., $t_{ID}^* = 154$ and 160 h along b or c in the 144 h simulations) or much longer ($t_{ID}^* = 151$ and 297 h along a in the 72 and 144 h runs, respectively, or a relative difference of +110%).

These observations argue for an important control of crystal shape on calculated diffusion times, interpreted here to be caused by merging element flux from multiple directions. In other words, if a diffusion front advances perpendicular to a given crystal face, then two diffusion fronts perpendicular to two faces at an angle lower than 180° from each other will merge (cf. Supplementary

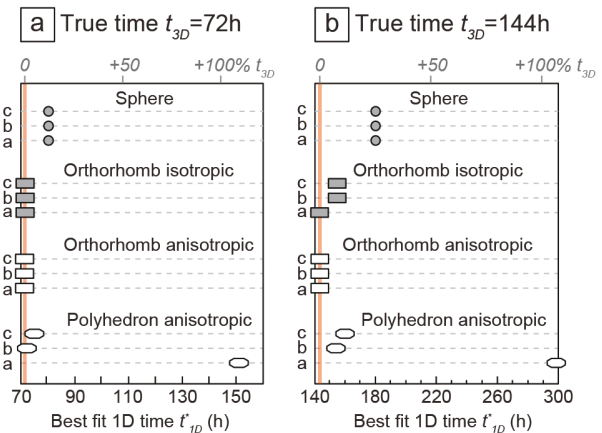


FIGURE 4. Influence of crystal morphology on timescales recovered from along-axis, on-center 1D models (i.e., a , b , or c axes). (a) Best-fit 1D times for different crystal shapes as a function of crystallographic axis for a true diffusion time $t_{3D} = 72$ h. (b) Same but for $t_{3D} = 144$ h.

Material¹). Thus, diffusion fronts in an olivine with sets of parallel faces (orthorhombic morphology) will generally not intersect in transects collected away from the corners, leading to accurate timescale predictions (see Supplementary Material¹). With increasing duration, however, the diffusion fronts originating from different crystal faces may reach the core via the shortest crystal dimension (the a -axis), generating differences between 1D and 3D along the other crystal dimensions, b and c . Compared with orthorhombic morphologies, polyhedral crystals typically have more faces meeting at angles $<180^\circ$, thus promoting interacting diffusion fronts and leading to systematic differences between 1D and 3D times, even along perfectly oriented transects (Appendix Fig. 4¹). The roughly twofold overestimate in 1D times along a in polyhedral models is a good example: the diffusion fronts originating from $\{110\}$ converge or diverge (depending on whether Fe or Mg is considered) from/toward the profile passing through the crystal center along the a -axis, resulting in interactions that cannot be modeled in 1D (Appendix Figs. 3¹ and 7¹). Finally, the surface of a sphere can be considered as an infinite combination of planes at a certain angle from each other, supporting the notion that even perfect sections or profiles across a sphere never produce the same results in 1D.

Along-axis, off-center sections. For all non-spherical morphologies, concentration profiles could be sampled along a given axis using two possible planes (e.g., the a - b or the a - c for along- a profiles). Here, the plane allowing for the longer sampling distance from the core was chosen (e.g., a - c was selected over a - b for the a -axis, b - c selected over a - b for the b -axis, and b - c chosen over a - c for the c -axis, Fig. 5). Furthermore, for off-center transects, the initial composition may only be apparent (i.e., different from the true initial Fo) (Costa and Chakraborty 2004; Costa et al. 2008). There are two possibilities to run the models: (1) using the true initial composition known from the 3D model, or (2) using the apparent extremum composition displayed by the off-center profile (the maximum or minimum Fo concentration, depending on whether zoning is normal or reverse). We initially tested the two possibilities for the spherical model (Fig. 5a). Using the initial composition as known, the difference between the true and the best-fit diffusion times ($\Delta t_{1D-3D} = t_{1D}^* - t_{3D}$) increased from +40 to +800 h (or +25 to +550% relative) with increasing sampling distance from the crystal center, until roughly 20 μm from the sphere edge. Then, closer to the edge, Δt_{1D-3D} decreased abruptly. In contrast, if the initial concentration was taken as the observed maxima or minima Fo in the diffused profile, the 1D-3D discrepancy was smaller, with values of $\Delta t_{1D-3D} = +200$ h (or +140% relative) about 45 μm from the crystal edge, and decreasing thereafter to negative values (i.e., 1D timescales became shorter than 3D). For the orthorhombic and polyhedral crystal, we took the initial concentration as observed (case B above). Orthorhombic models showed excellent agreement between 1D and 3D times ($\Delta t_{1D-3D} = 0$) up to distances ~ 160 μm from the core for transects performed along the a and b axes, and up to ~ 80 μm for those selected along the c axis. Closer to the crystal edges, Δt_{1D-3D} increased to +25–50 h depending on whether diffusion anisotropy was accounted for (Figs. 5b and 5c). We note that contrary to spherical models, Δt_{1D-3D} did not decrease noticeably as transects were sampled closer to the crystal faces. Polyhedral models yielded the most variable timescales (Fig. 5d).

From the core to about ~ 140 μm , transects sampled along the a -axis systematically gave time overestimates ($\Delta t_{1D-3D} = +150$ h or +105%). Closer to the edge, 1D times underestimated the true diffusion time ($\Delta t_{1D-3D} = -115$ h or -80%). Concentration profiles taken along the b -axis showed good correspondence between 1D and 3D close to the core, rapidly degrading to values $\Delta t_{1D-3D} = +100$ –700 h at distances larger than 40 μm , then decreasing to negative values at the crystal edge. In contrast, transects along c produced timescales that agreed better with the known diffusion time. The topology of profiles obtained in polyhedral crystals were similar to those from the orthorhombic model along a , but closer to that of spherical models along b and c .

The effects of sampling distance from the core and choice of initial concentrations on calculated timescales can be interpreted as follows: if the initial Fo concentration is known, shortening of the profiles with increasing distance from core leads to longer calculated times, as the model requires additional total element transfer to reach the same final concentration gradient (cf. Supplementary Material¹). With increasing distance from the center, however, this shortening induces a decrease in calculated times because the apparent element transfer becomes very small. This trade-off between profile length and element transfer required to attain a given concentration explains the increase and subsequent decrease in best-matching 1D times with increasing sampling distance from the core of spherical crystals (Fig. 5a). If the observed Fo extremum is chosen as the initial value, the same trade-off is observed, although a much smaller total flux is required to reach the final profile (Figs. 5a–5d), potentially leading to shorter calculated times and even time underestimates closer to the crystal edge (Figs. 5a and 5d). Overall, we emphasize that models employing the polyhedral shape display the most complex behavior with respect to transect distance from core, with no apparent systematic shifts in time mismatch common to the three sampling directions.

Randomly oriented, on-center sections. To isolate the influence of diffusion anisotropy from that of crystal geometry, the models were first run assuming isotropic diffusion (using $D = D_e$), and later incorporated the anisotropy correction (Eq. 4). Because transects were collected within sections passing through the core, the initial Fo concentration was generally preserved, except for the isotropic rectangular models run for 144 h, in which the core composition was slightly affected.

Sections obtained by slicing crystals through their cores generally showed a high degree of symmetry, with matching concentration gradients for faces of the same form (e.g., $\{110\}$ and $\{021\}$, Figs. 6a and 6b). Sets of traverses selected across opposite crystal faces displayed a similar topology, and anisotropy-corrected 1D models yielded timescales close to the true time (Fig. 6a). On the other hand, transects taken across section corners (Fig. 6b), despite maintaining fairly good symmetry, resulted in large time overestimates. Thus, for the rest of this study, all 1D models were sampled away from corners in a given olivine section (however note that the section may still have been close to an edge or corner in the third dimension).

Two-hundred 1D models performed in orthorhombic crystals (isotropic diffusion) displayed minor time mismatches for profiles taken perpendicular to the crystal faces (Fig. 7a). In comparison, oblique transects and those collected toward edges

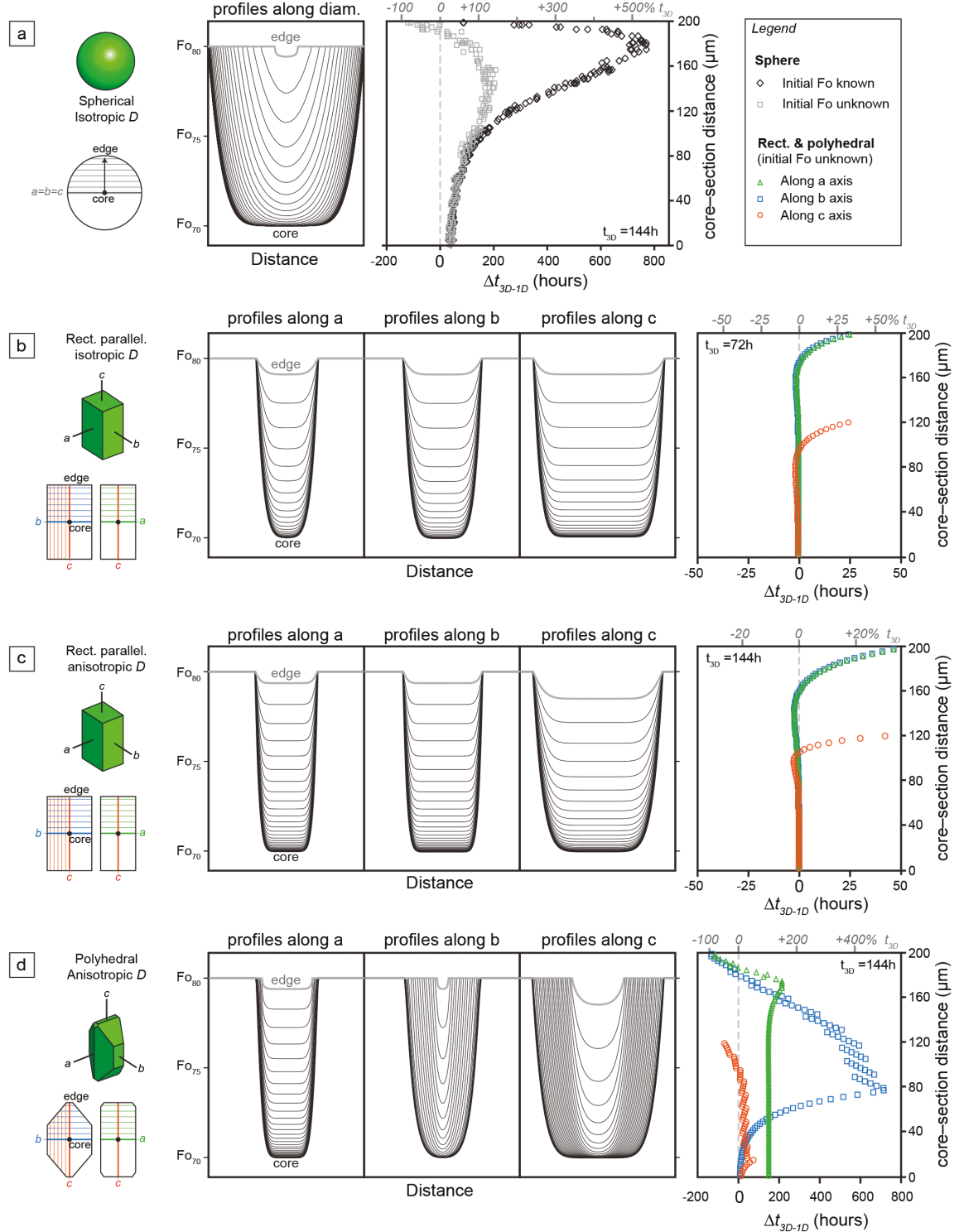


FIGURE 5. Influence of sectioning distance from the core for the three crystal shapes. **(a)** Sphere: profiles are sampled from the 3D model after diffusion for $t_{3D} = 144$ h at increasing distances from the core (illustration at the bottom left). The difference between the true (3D) and best-fit (1D) times to each profile is plotted against distance from the core (plots at the right), both as absolute (hours, bottom x-axis) and relative (% top x-axis). Two scenarios are examined for the spherical morphology, one where the initial concentration profile is the known 3D initial profile (“Initial Fo known”), the other using the apparent observed minimum Fo content (“Initial Fo unknown”). **(b) to (d)** Similar plots for the orthorhombic and polyhedral crystals using isotropic (**b**) or anisotropic (**c** and **d**) diffusion coefficients, sampled along each of the three crystallographic axes. For these models, the initial Fo was taken as the apparent minimum value. Note that the orthorhombic model using an isotropic D was only run for 72 h so as to avoid affecting the concentration at the core (also see Supplementary Material’).

and corners typically produced time overestimates $\Delta t_{1D-3D} > +100$ h (with a maximum of +750 h, or +520% the true time). Similar models incorporating anisotropic diffusion showed good agreement between 1D and 3D times for profiles that were perpendicular to crystal faces (Fig. 7b). Edges or near corner transects result in time underestimates $\Delta t_{1D-3D} < -20$ h (−15%), while transects that are oblique to crystal faces also gave overestimates $\Delta t_{1D-3D} > +20$ –100 h (+15–70%). For polyhedral morphologies with anisotropic diffusion, the best time estimates were still derived from transects perpendicular to crystal faces (Fig. 7c). Transects oriented close to the a , b , and c axes resulted in $\Delta t_{1D-3D} > +20$ –100 h, the worst cases were for profiles parallel to a and at slight angles from b and c .

We attribute the emergence of time underestimates, which only appear in the anisotropic 1D models (Figs. 7b and 7c), to the fact that several transects are not sampled perfectly parallel to the concentration gradient in all 3 dimensions. Along these directions, the anisotropy correction expression (Eq. 4) tends to overcorrect diffusivities (e.g., Supplementary Material¹). These time underestimates are indeed clustered near crystal edges (orthorhombic crystal, Fig. 7b) or crystal faces that are oblique to the main diffusion axes (polyhedral crystal, Fig. 7c). On the other hand, time overestimates typically result from artificial lengthening of the concentration gradients. This lengthening may be caused by either sectioning a concentration gradient at an angle, and/or sampling locations affected by diffusion front interactions (corners and edges) (Figs. 7a, 7b, and 7c).

The consequences of adding section orientation as a free parameter in our simulations was also examined by displaying the same models as time-frequency histograms (Fig. 8). Timescales all fell within the 180–220 h range with a mode at $t_{1D}^* = 200$ h (+40% the true 3D time of 144 h; Fig. 8a). In contrast, isotropic models from orthorhombic crystals produced a broad distribution with a mode at $t_{1D}^* = 140$ h, heavily skewed toward high values (up to 875 h or +500% the true time, Fig. 8b). The 1D models with no D -correction replicated timescales produced by the

orthorhombic models that incorporated anisotropic D poorly, with a bimodal time distribution (modes at $t_{1D}^* = 40$ and 140 h). Correcting for D in these models resulted in a mostly unimodal distribution (mode at $t_{1D}^* = 140$ h and shoulder at 80 h), with a wide range of times $69 < t_{1D}^* < 490$ h (Fig. 8c). Polyhedral crystals yielded trimodal distributions (modes at $t_{1D}^* = 20$, 80, and 160 h) for uncorrected D , while the same models generated unimodal, positively skewed distributions when the correction was applied (mode between $t_{1D}^* = 120$ –140 h and range of timescales $86 < t_{1D}^* < 460$ h; Fig. 8d).

Overall, if we do not correct for anisotropy in 3D models we find multimodal time distributions. The number of modes largely depends on the probability that a transect is taken across a given set of faces. For orthorhombic crystals (Fig. 8c), uncorrected bimodal time distributions correspond to the main diffusion directions: the mode at short times $t_{1D}^* = 20$ h (−85% the true time) can be associated with profiles taken along the slower a and b axes (i.e., across faces belonging to the {100} and {010} forms), and the mode around the true 3D time $t_{1D}^* = 140$ h corresponds to those collected along the faster c -axis profiles (i.e., across {001}). The well-defined third mode in polyhedral crystals (Fig. 8d) probably corresponds to transects taken across the prismatic faces of the olivine (i.e., faces belonging to the {110} or {021} forms, cf. Fig. 2a), which are absent in the rectangular shape.

Randomly oriented, off-center sections. The effects of random sectioning were first examined on a single section. Compared with center-cut crystals (Figs. 6a and 6b), an off-center section often showed asymmetrical concentration gradients across the different faces (Fig. 6c). Diffusion models performed using four such transects produced timescales that span a wide range $t_{1D}^* = 72$ –989 h (−50 to +590%), with important time under- and overestimates.

Unlike previous cases where crystal sections were along-axis off-center (Fig. 5) or on-center but randomly oriented (Figs. 7a, 7b, and 7c), identifying systematic behaviors when both orientation and off-center distance are randomized was more difficult

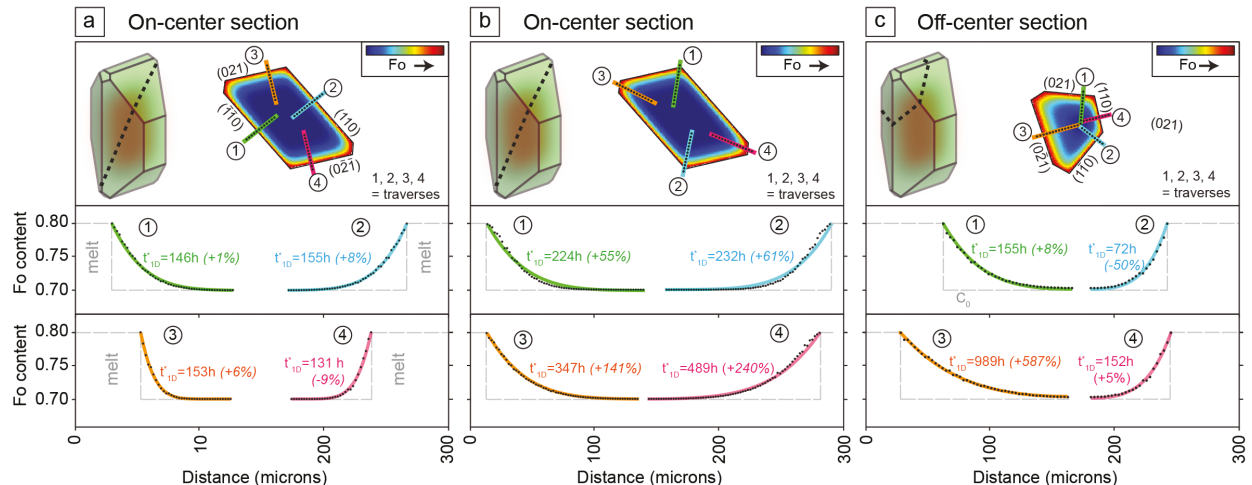


FIGURE 6. Topologies of concentration profiles sampled from (a and b) sections passing through the crystal core, and (c) an off-center section. For each case, the top illustration displays the section and the traverse locations, and the bottom plots show the corresponding Fo profiles and best-fit 1D diffusion times (absolute and relative). In all models, the diffusion coefficient D has been corrected for anisotropy to isolate the influence of section location from anisotropy.

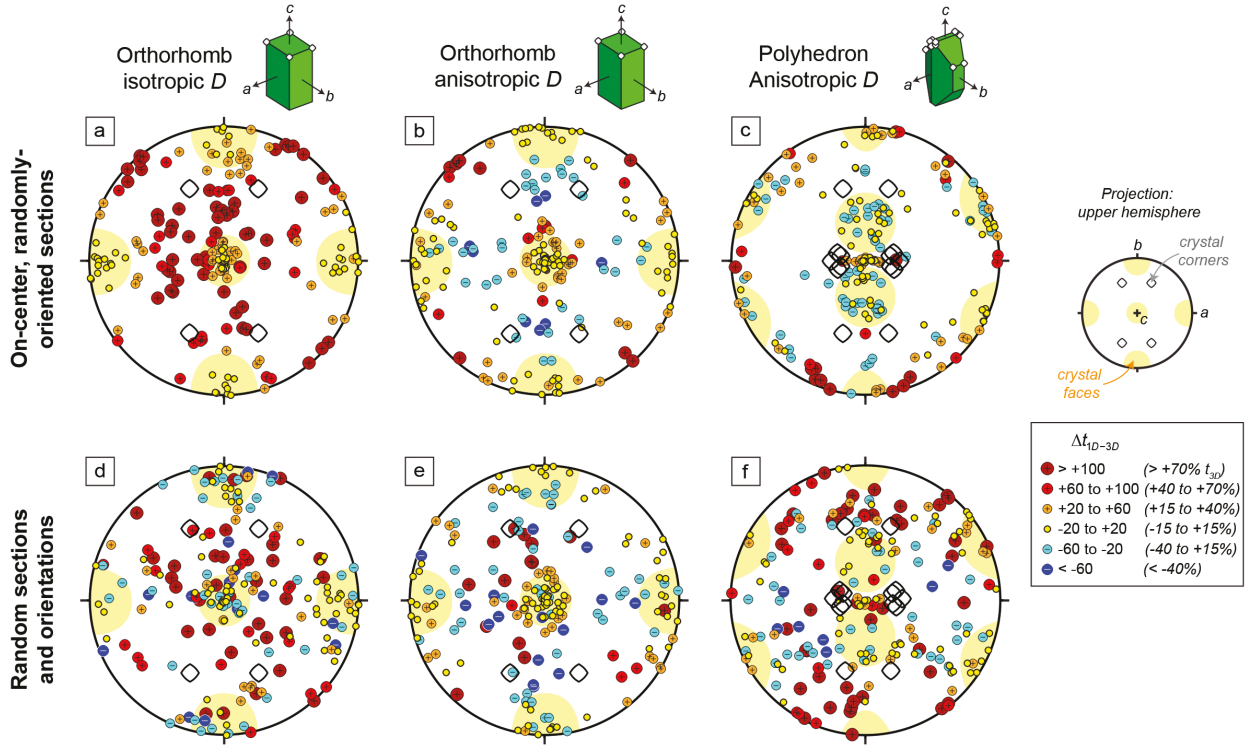


FIGURE 7. Effects of concentration profile orientation on calculated 1D diffusion times for transects collected along the crystal center (top row) and for transects sampled at random distances from the core (bottom row). Data are displayed as pole figures (equal-angle stereographic projections, plotted using Stereonet 9 by Cardozo and Allmendinger 2013), with the locations of crystal faces and corners indicated as yellow areas and large hollow diamonds, respectively (see small inset on the right). In all cases, the real diffusion time is $t_{3D} = 144$ h and 1D model misfits are represented as a color-coded difference Δt_{1D-3D} , with symbols containing a “plus” and “minus” sign being associated with time over- and underestimates, respectively. (a) Orthorhombic crystal with isotropic D , (b) orthorhombic crystal with anisotropic D , and (c) polyhedral crystal with anisotropic D . (d, e, and f) These are the same but allowed for off-center sectioning. All the models in this figure used the apparent observed extremum Fo as the initial concentration, which may or may not correspond to the true initial Fo (i.e., for on or off-center sections, respectively).

(Figs. 7d, 7e, and 7f). Compared with center-cut models (Fig. 7a), transects sampled from off-center sections in orthorhombic crystals with isotropic D (Fig. 7d) showed a less well organized distribution of time overestimates with respect to orientation, in addition to producing time underestimates. Orthorhombic crystal runs using anisotropic D (Fig. 7e) also resulted in time underestimates more frequently compared to the center-cut version (Fig. 7b). Finally, off-center polyhedral models displayed much more randomness in the distribution of timescales with respect to transect orientation (Fig. 7f).

When shown on time vs. frequency histograms, spherical crystals (Fig. 8e) displayed a clear mode at $t_{1D}^* = 180$ h (range of 180–912 h, or +25 to +530% the true time of 144 h) rapidly decaying toward high values when the initial Fo concentration was set to the known initial value (Fo_{70}). Imposing the apparent observed Fo concentration as the initial value eliminated the 1D times greater than 400 h, but generated a few models with much lower durations with $t_{1D}^* = 20$ h (~85% relative). New secondary modes also appeared at $t_{1D}^* = 220$ and 300 h. Distributions from orthorhombic crystal simulations with isotropic D are unimodal (Fig. 8f), the mode corresponding to the 3D time only when the initial Fo is taken as the apparent measured value. Anisotropic models using a rectangular or polyhedral geometry yielded bi- to

trimodal distributions with modes at $t_{1D}^* = 20$ h when a unique value of D is used, while those that are corrected for anisotropy gave mostly unimodal curves with modes at $t_{1D}^* = 140$ h (Figs. 8g and 8h).

Globally, when initial concentrations are lost due to sectioning, models that use the extremum Fo as an initial value produce timescales that may underestimate or overestimate the true value by factors of 4–5 (Figs. 5, 8e, and 8f). If instead the known initial profile is used, timescales are typically longer, and do not show any improvement on overall accuracy (Figs. 5a, 8e, and 8f). In most cases the apparent measured Fo is used as initial concentration since in practice, estimating the composition before diffusion occurred is not straightforward; these results demonstrate that when initial compositions are lost due to sectioning effects, using the measured apparent Fo can actually be better than using the true initial composition, which is a counterintuitive result.

In summary, models testing the influence of section orientation and position on timescales show some trends (Figs. 5, 7a, 7b, and 7c), but mainly complex patterns, particularly for olivines with realistic shapes (e.g., Fig. 7f). Profiles near the edge of a 3D crystal always result in inaccurate 1D timescales, independent of section orientation.

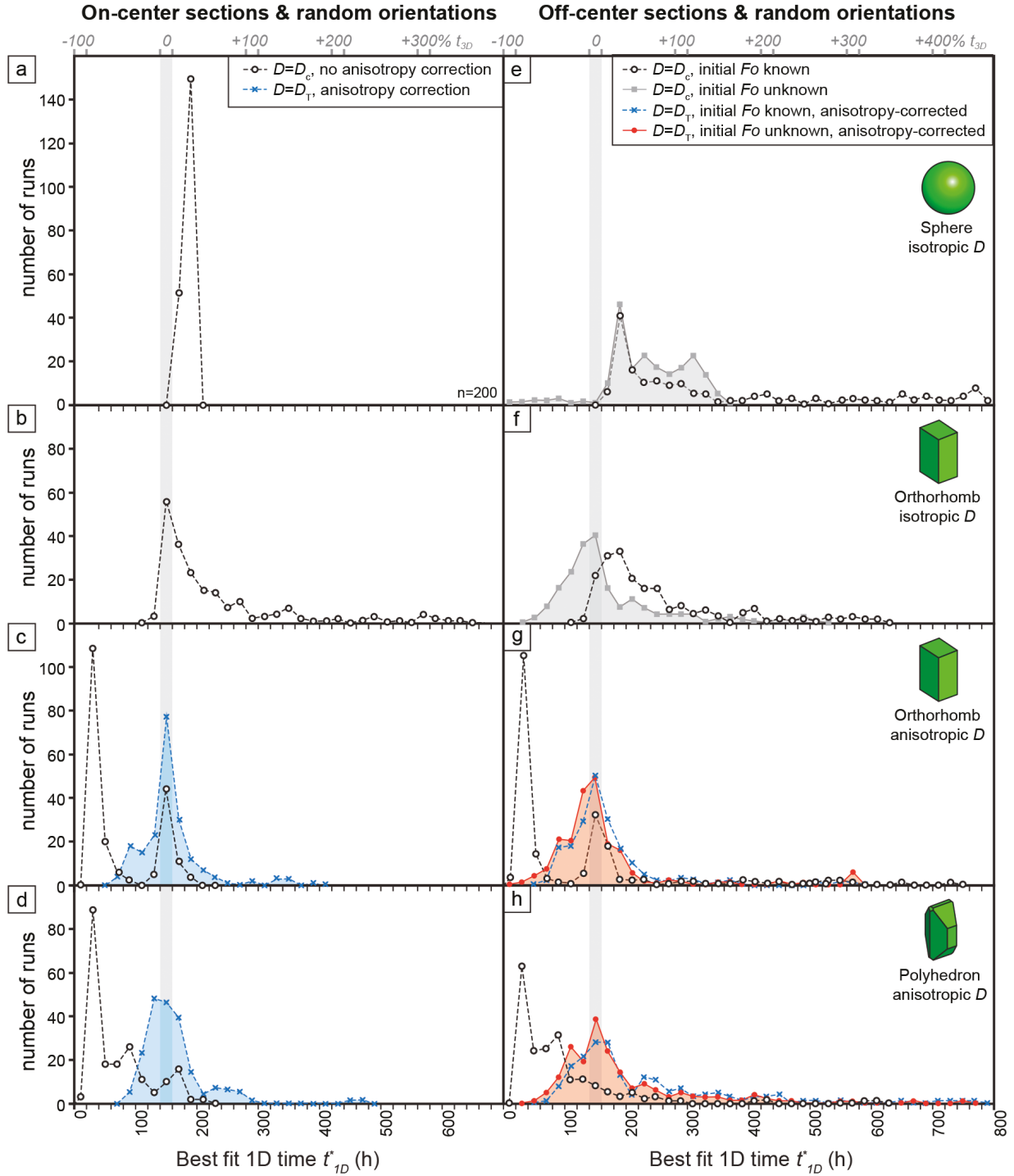


FIGURE 8. Distribution histograms of best-fit 1D timescales for 200 randomly oriented, on-center models (left plots), and randomly oriented, off-center models (right plots). Four different distributions are shown, corresponding to models performed without anisotropy correction and with the known initial Fo profile assumption (black symbols), with isotropic D and an “unknown” initial Fo profile (using the apparent minimum Fo) (gray), with anisotropy correction and a known Fo profile (blue), or with anisotropy correction and an unknown initial Fo profile (red). For each of the spherical (**a** and **e**), orthorhombic (**b**, **c**, **f**, and **g**), and polyhedral (**d** and **h**) morphologies, the most accurate distribution is shaded according to the parameters assumed (gray, blue, or red). The vertical gray band marks the true 3D diffusion time of 144 h and the top x-axis marks correspond to the relative time difference.

INFLUENCE OF ZONING CONFIGURATION

We also examined the role of zoning style on the timescale distributions obtained from 1D models collected along random orientation and/or distances from the olivine core. Additional sets of 1D and 2D models performed along principal sections and crystal axes were also carried out to examine whether such ideal locations are better or worse for timescale extraction, and are presented in the Supplementary Material¹.

Randomly oriented, on-center sections. Zoning style seems to have little effect on the distribution of timescales when sections were sampled on-center but along random directions (Fig. 9a). For the 6 zoning styles examined, models that did not take into account diffusion anisotropy generally produced trimodal distributions with modes at $t_{1D}^* = 20$ h, 60 h, and around 120–160 h (at –85, –60, and –15 to +10% relative). The distributions became mostly unimodal (except for the core-rim I configuration, which has two apparent modes) and centered on the true time when we corrected for diffusion anisotropy. Maximum timescales calculated range from 300 to 400 h (+110 to +180% of t_{3D}). It should be noted that after a duration $t_{3D} = 144$ h, core-rim zoning types II and III (normal-reverse and reverse-normal, respectively) did not preserve the initial Fo concentrations at the core or at the rim (see Supplementary Material¹). The initial rim compositions were erased after merely 12–24 h within core-rim model II. For these center cut sections, however, there is little difference between the accuracy of timescales retrieved at $t_{3D} = 12$ h or $t_{3D} = 144$ h (i.e., both have unimodal distributions centered on the correct time).

Overall, incorporating random section/profile orientation into the simple zoning models (Fig. 9a) still allows for accurate diffusion timescale predictions in 1D, provided that the anisotropy of diffusion is accounted for. This implies that the large mismatches encountered along a (Figs. 4a and 4b) are an exception. However, even with anisotropy correction, some 1D models actually underestimated the true time because D was likely over-corrected in certain combinations of section orientation and sampling directions (also see Fig. 7). The time distributions produced from core-rim zoning types are fairly similar to simple normal- or reverse-zoned runs (Fig. 9a), with, nevertheless, a more prominent secondary peak of timescales underestimates.

Randomly oriented, off-center sections. For the six zoning styles, three types of simulations were examined: (1) no diffusion anisotropy correction and the initial Fo content was known; (2) the same as no. 1 but with correction for diffusion anisotropy; and (3) with diffusion anisotropy correction and initial Fo taken as apparent observed extremum value.

Similarly to the center-cut models, off-center models uncorrected for diffusion anisotropy always displayed multimodal distributions (Fig. 9b). Also like center-cut models, simulations performed using anisotropy-corrected diffusion coefficients gave mostly unimodal distributions, with tails of longer durations, whether initial Fo was known or not. For the three simple crystal-melt zoning configurations (normal I, normal II, and reverse), as well as for the core-rim I scenario, knowledge of the initial composition had a minor effect on the shape of the distributions or on the position of the main distribution mode, systematically located at the true time $t_{1D}^* \approx t_{3D} = 140$ h. In contrast, knowledge of initial Fo strongly influenced the location of the primary mode for zoning configurations core-rim II and III: if the initial

composition was known, the distribution modes agreed with the true diffusion times, but if the initial Fo was taken as the apparent observed composition, those modes shifted toward lower timescales $t_{1D}^* = 60$ h (~60% relative). This discrepancy arises from diffusive loss of the initial core and rim concentrations in the 3D models, meaning that apparent extremum concentrations used as initial profiles for 1D models are very different from the real initial concentrations and result in unrealistic timescales (see Supplementary Material¹). In general, nevertheless, possessing information on initial concentrations resulted in broader time distributions than when information on initial Fo was lacking. For the core-rim I model, for example, 1D diffusion times reached values up to 1440 h (+900% of t_{3D}) when the initial Fo was known, while maximum values only attained 540 h when the apparent observed Fo was used.

In summary, when off-center sections were allowed in the simulations, the narrow time distribution previously obtained for on-center sections (Fig. 9a) became wider in both longer and shorter times, and gained a large tail toward longer timescales (Fig. 9b). The time overestimates mostly stemmed from off-center sections (Fig. 5), as well as orientations that favor locations of diffusion front interactions (Fig. 7). For core-rim models sectioned randomly after $t_{3D} = 144$ h (Fig. 9b), the contrasting tendency for 1D time distributions to shift toward lower timescales can be ascribed to a loss of initial concentrations both at the rim and at the core. Therefore, overall, poor quality timescales were obtained from models with core-rim zoning patterns that no longer displayed compositional plateaus.

DISCUSSION

In the following sections, we successively discuss the importance of considering spatial dimensions, compositional plateaus, diffusion anisotropy, and crystal morphology for applications aiming to extract timescales from diffusion modeling. Finally, we also examine the extent to which these considerations may apply to other elements and minerals.

Sectioning zoned crystals: Perspectives from the three dimensions

Irrespective of the specific crystal morphology, and whether diffusion is isotropic or not, it is very important to consider the effects of three dimensions in kinetic modeling. Pearce (1984) demonstrated that randomly sampling a zoned equidimensional olivine leads to various concentration profiles, from perfectly symmetrical to largely asymmetrical, from short to long (in terms of transect dimension along x), and with preservation or loss of initial compositional plateaus. Our 3D models confirm the variability of concentration profiles obtained by sectioning, particularly for those that are collected far from the core.

Costa et al. (2003) and Costa and Chakraborty (2004) incorporated 2D models within their investigation of diffusion in plagioclase and olivine to investigate the dimensional effects on retrieved timescales. For both types of minerals, they sampled the concentration profiles parallel to the crystallographic axes, and found that ignoring the element flux originating from other dimensions can lengthen the 1D-derived times by a factor of three if the profiles are taken on-center, and by a factor of five off-center. These conclusions are supported by our models, with

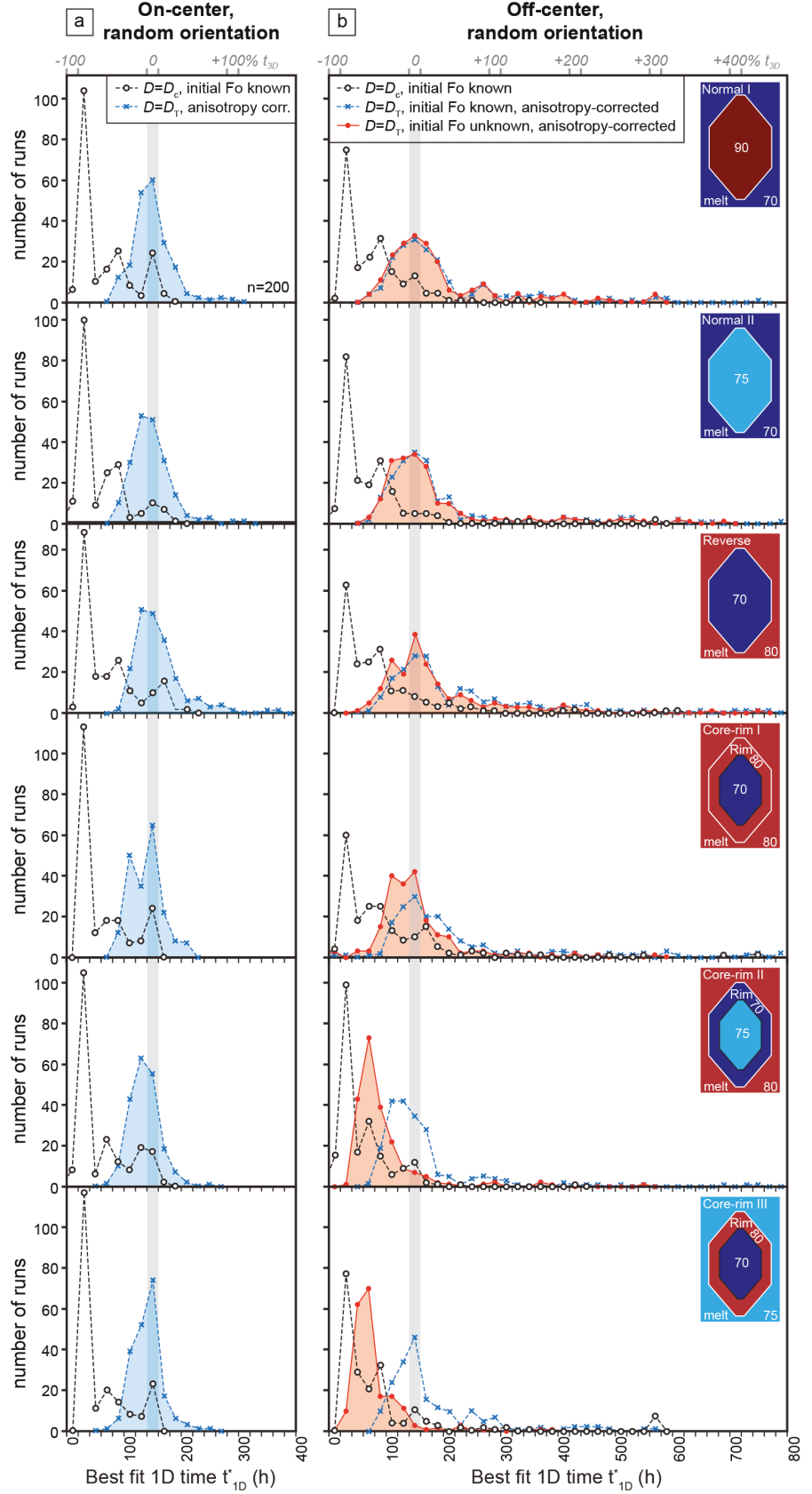


FIGURE 9. Distribution histograms for 200 models testing various initial zoning configurations. The reference 3D model has a true diffusion time $t_{3D} = 144$ h. Distributions obtained for (a) on-center, randomly oriented models, and (b) off-center, randomly oriented models. Black symbols designate the set of models performed using a single D value, while blue symbols represent models corrected for D anisotropy. Distributions in red symbols correspond to anisotropy-corrected runs with no a priori knowledge of the initial concentration profile (“unknown Fo”). Gray vertical arrays mark the true 3D times.

the added complexity that when the core Fo content is lost or the crystal geometry is non-rectangular (i.e., with narrowing across-crystal distances away from the core, Fig. 5), simulations may actually underestimate the true times. Whether the diffusion times are under- or overestimated in these cases depends purely on the apparent total mass transferred, and the direction of this discrepancy is hard to anticipate.

The role of initial concentration plateaus

In our study we focused on applying realistic initial boundary conditions (i.e., using the extremum observed concentration to build the initial Fo profile), and also explored cases where the true initial concentration was known. Interestingly, for simple zoning patterns (i.e., normal or reverse without rim), knowledge of the initial Fo was not advantageous for retrieving accurate timescales, as the 1D-3D time differences typically worsened in cases where we used the known initial composition. This is because in the initial 3D model, off-center locations will transfer Fo more rapidly than toward the core, and ascribing the “true” initial Fo to a 1D model artificially lengthens the total diffusion time. When the initial concentration has been lost to a significant extent at the core or at the rim, however, timescales are typically underestimated (see Supplementary Material¹). In these situations, calculations of diffusion times should be tested for various plausible initial core and/or rim concentrations to determine potential uncertainties. An alternative approach used to infer the topology of the initial concentration for olivine or other phases such as plagioclase, is to measure slow-diffusing elements (e.g., Ca, P, or Al in olivine, CaAl-NaSi in plagioclase) concurrently with the elements of interest (Costa et al. 2003; Milman-Barris et al. 2008; Kahl et al. 2011; Druitt et al. 2012). A relationship between the main diffusing elements and the slow diffusers is calculated, and the initial concentration can be inferred. This type of calculation works if the crystal grew in near equilibrium conditions (e.g., using the melt P and the Fo component in olivine or Mg and An component in plagioclase) (e.g., Albarède and Bottinga 1972; Costa et al. 2010; Ruprecht and Plank 2013), yet sufficiently rapid compared to diffusion that the diffusive re-equilibration is distinct from growth.

An imperfect but adequate anisotropy correction

The equation used to correct for diffusion anisotropy (Eq. 4) requires knowledge of section orientation with respect to the crystallographic axes, which is readily obtainable using electron backscatter diffraction (EBSD) analysis (Prior et al. 1999; Costa and Chakraborty 2004; Costa and Dungan 2005; Hammer et al. 2010; Kahl et al. 2011; Sio et al. 2013). Without this correction, calculated timescales are likely to be inaccurate and imprecise (e.g., Fig. 8). Even when D is anisotropy-corrected, and sections are taken along the crystal center, 1D models do not result in a single timescale, but rather in a distribution around the true 3D time. This issue occurs because Equation 4 is strictly applicable to transects perfectly parallel to the concentration gradient, which is not necessarily the case in our simulations (or in nature) despite appearing parallel on a section. The geometrically correct, generalized equation is not easily applicable in practice since concentration variations in the third dimension are not known. The rapidly advancing field of X-ray micro-tomography analysis

may allow an accurate 3D characterization of Fo in olivine in the near future (e.g., Pankhurst et al. 2014). Until then, using the simpler anisotropy correction formula already improves the accuracy and precision of timescales considerably.

We note that the quality of 1D model fits from uncorrected D are just as satisfactory as those obtained using a corrected D , implying that the goodness of fit is not necessarily a solid indicator of the timescale accuracy. Recent works have derived timescales in anisotropic minerals using diffusion coefficients along the slowest and/or the fastest crystal directions, and argued that those provide minimum or maximum estimates, or potentially encompass the possible range in diffusion times (e.g., Pan and Batiza 2002; Ruprecht and Plank 2013; Longpre et al. 2014). However, even when using the fastest diffusion coefficient D_c , our randomly sectioned crystals with real diffusion times $t_{3D} = 144$ h yielded best-fit 1D durations of anywhere between 10–600 h (cf. Fig. 9). Using the slowest diffusion coefficient D_a ($= D_b$) would change this range by a factor of 6 (i.e., 60–3600 h). Therefore, without correcting for diffusion anisotropy, calculated timescales from randomly sectioned olivines can actually span anywhere from ~ 0.1 – $25\times$ the true diffusion time.

Importance of considering crystal morphology

Multidimensional effects on calculated times are generally examined using simple geometries and analytical solutions (i.e., spheres, cylinders, and rectangular parallelepiped; Pan and Batiza 2002; Costa and Chakraborty 2004, 2008; Watson et al. 2010), but the addition of morphological complexity of natural crystals combined with random sectioning during thin section preparation affects the calculated timescales considerably.

The results from our numerical models involving randomly sectioned spherical crystals yield longer timescales (cf. Fig. 8) is opposite to that observed by Pan and Batiza (2002), who found that calculated times exponentially decreased toward small values, presumably as sections were sampled away from their centers. Such shorter times were rarely obtained in our simulations because the length of an apparent concentration gradient in a given random transect is always equal or longer than the true concentration gradient length. Only in cases where the transect width shortened closer to the edges did 1D diffusion times underestimate the true time in spherical models (Fig. 5).

For other geometries (rectangular and polyhedral), the convergence of diffusion fronts from different faces typically results in a longer apparent concentration gradient, and whether 1D modeling of such gradients yields shorter or longer timescales also depends on the relationship between apparent composition (whether initial plateaus are preserved or not) and the apparent width of the profile across the crystal. Zones of interacting diffusion fronts, typically crystal corners, are not good for kinetic modeling of timescales.

Relevance of results for other elements, crystal shapes, and minerals

The diffusion and crystal sectioning exercise we have done for Fe-Mg in olivine is also relevant for other elements, such as Ca, Ti, V, Cr, Mn, Co, and Ni since they also show diffusion anisotropy (faster in the c direction; e.g., Petry et al. 2004; Coogan et al.

2005; Chakraborty 2010; Spandler and O'Neill 2010). Moreover, the provisions dictated by dimensional, interacting diffusion fronts and sectioning effects highlighted above will also apply.

The polyhedral morphology we have used contains the most common crystal faces of olivines crystallizing in the laboratory or in nature (e.g., Faure et al. 2007; Welsch et al. 2009, 2013). Nevertheless, even this fairly archetypal olivine can appear in a wide variety of aspect ratios, which will presumably influence where the zones of interacting diffusion fronts occur, in addition to the rate at which the crystal core concentration will be affected by the diffusion process (e.g., the short axis of a highly elongate olivine). Even more complex morphologies resulting from rapid growth (e.g., spinifex, skeletal, or dendritic; Bryan 1972; Faure et al. 2003, 2006; Shea and Hammer 2013; Welsch et al. 2013) will host more regions of interacting diffusion fronts; therefore additional caution is warranted when attempting to perform 1D diffusion modeling in such crystals. Our models involving spherical shapes also displayed departures from the true diffusion times; olivines that have rounded rather than faceted habits are thus also susceptible to providing less accurate results.

Diffusion modeling of elements has also been recently used in feldspars (e.g., Mg, Sr, Ba) and pyroxenes (e.g., Fe-Mg) to decipher timescales of magmatic processes (e.g., Costa et al. 2003; Morgan et al. 2004, 2006; Cherniak 2010; Druitt et al. 2012; Saunders et al. 2012; Ruprecht and Cooper 2012). Diffusion anisotropy for most elements in these minerals is not well characterized or appears to be moderate and should not be an important source of uncertainty in calculated times. Other issues of merging diffusion fronts and added flux from other dimensions identified in this study are nevertheless expected to apply to feldspars and pyroxenes in the same fashion.

IMPLICATIONS

Which sections/profiles are most adequate?

While a suitable correction can be applied for diffusion anisotropy in olivine, there is no general quantitative adjustment to correct for problems associated with crystal sectioning or dimensional effects because their influence on calculated timescales is too dependent on morphology (number and relationship between

faces, aspect ratio, and roundness). Consequently, rather than attempting to find a posteriori empirical corrections for intersection and third dimension issues, attention should be focused on identifying the best suitable sections for diffusion modeling. In their investigation of diffusion in natural garnets, Ganguly et al. (2000) noted that uncertainty in calculated timescales can partly derive from the profile not being perfectly parallel to the 3D concentration gradient. Our results support this notion, although the influence of less-than-perfect transect orientation on retrieved timescales is less important than not correcting for anisotropy or other sectioning and/or second and third dimension effects (i.e., diffusion front interactions). Typically, the largest errors appear in sections that are oblique to crystal faces and generate extended concentration gradients. Such gradients are rarely observed in center-cut sections but much more common in highly off-center cuts. Because off-center sections often intersect sets of faces at very different angles, they also result in apparent concentration gradients with different widths from face to face, and thus often asymmetric. Yet another related symptom of off-center cuts is the presence of dipping plateaus in the observed gradients (also see Pearce 1984), and even in certain cases, the absence of any compositional plateau despite the fact that diffusion has not reached the crystal core (also see Costa et al. 2003; Costa and Chakraborty 2004).

Aside from problems of intersections, crystals that have no compositional plateau at the core (or at the rim in the case of more complex zonings) are more susceptible to give inaccurate timescales (both under- and overestimates are possible, Supplementary Material¹) because they are likely to be: (1) either sectioned largely off-center, in which case using the apparent observed extremum composition as initial is no worse than knowing the initial concentration, or (2) sectioned through their center but having diffused long enough to lose the initial concentration. Nonetheless, if no better sections are available, an analysis of timescale variability and goodness-of-fit as a function of initial concentration can be carried out.

We also showed that profiles measured across crystal regions containing corners or near face intersections are likely to yield incorrect timescales due to interacting diffusion fronts. While one it is difficult to ensure that a given section does not cut through such a region, it is at least possible to select a profile away from

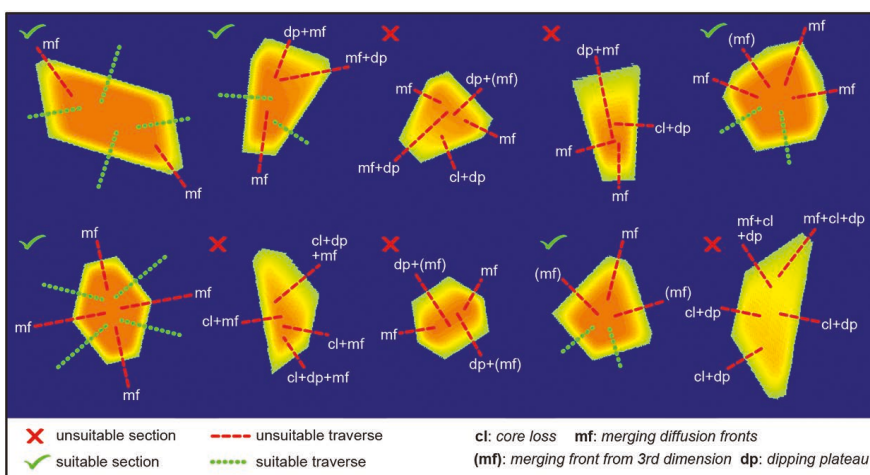


FIGURE 10. Choosing the right section and profile. Ten sections of a normally zoned olivine display various habits and concentration gradients. Green check marks and red crosses mark the suitability or unsuitability of each section for 1D diffusion modeling. Green and red dotted lines designate adequate and problematic profiles. Discarded profiles are labeled according to the various symptoms identified. Note that “(mf)” designates fronts originating from the third dimension, which would not be normally recognized in a section. For example, the two problematic profiles marked (mf) on the seventh section would likely be missed and considered appropriate for modeling.

any apparent face intersection. The same rule applies to any zones of the olivine displaying rounding.

In summary, when numerous crystals are available within a thin section, simple olivine selection guidelines can be followed (examples of suitable and unsuitable thin sections are given in Figs. 1 and 10). Note that it is assumed here that the work of identifying distinct populations with different crystallization/diffusion histories has already been performed (i.e., populations with different zoning styles, e.g., Pan and Batiza 2002; Costa and Chakraborty 2004; Kahl et al. 2011, 2013), and those guidelines apply to selection of the most suitable crystals within one such population:

(1) When looking for good crystals disregard the smallest ones, which have a higher probability of being off-center sections. Note that small sections may also be center cuts through smaller crystal populations (e.g., Saltikov 1967) since olivine sizes vary in real rocks. Even so, smaller populations are more likely to experience other issues (loss of initial concentration) and it is better to avoid them.

(2) Profiles should be obtained away from crystal corners and locations of obvious concentration gradient “rounding” since these regions likely experienced merging diffusion fronts. This means that complex morphologies (e.g., skeletal olivines) should be avoided for 1D modeling considering their propensity to host numerous crystal edges and corners. Polyhedral, nicely faceted crystals are therefore preferable. More complex morphologies can be used but 2D and/or 3D models are probably required to recover robust timescales.

(3) If possible, choose olivines that display a clear concentration plateau but discard those that display dipping plateaus, since they are highly off center and/or oblique cuts. Identifying these sections is straightforward for Fo zoning since acquiring back-scatter electron (BSE) images usually suffice to image relative variations in major element composition (see Supplementary Material¹ for examples). In any case, it is recommended to check for core compositions using energy-dispersive X-ray spectroscopy (EDS) spots or transects.

(4) Avoid olivine sections that completely lack any concentration gradient symmetry across the different faces (i.e., different gradient widths). Such cuts are often oblique to most faces and concentration gradients.

(5) If possible, find crystals that contain at least two suitable transect directions perpendicular to two different faces (cf. Fig. 10). Finding such sections can help: (1) verify that diffusion occurred anisotropically, and thus that gradients are not related to growth (Costa et al. 2008), and (2) test the variability of obtained timescales within a single olivine.

Providing that a sufficient number of crystal sections are available, these selection criteria are fairly easy to apply for modeling of Fo diffusion. The same is not necessarily true for trace elements since compositional variations are not resolved by BSE images. Nevertheless, the symptoms of unsuitable olivine sections will be the same, and the Fe-Mg content can still be used to perform the initial crystal selection process. Finally, once a set of adequate sections is identified, the analyst should determine grain orientation using EBSD (e.g., Costa and Chakraborty 2004) or other techniques such as microRaman (Ishibashi et al. 2008), since correcting for anisotropy is sine qua non to obtaining accurate 1D timescales.

WHAT IS THE ACCURACY AND PRECISION THAT CAN BE EXPECTED FROM 1D MODELING?

If the olivine selection criteria described above are applied to the sections obtained from the models in this study (100 olivine cuts, 2 traverses per crystal), the number of suitable sections

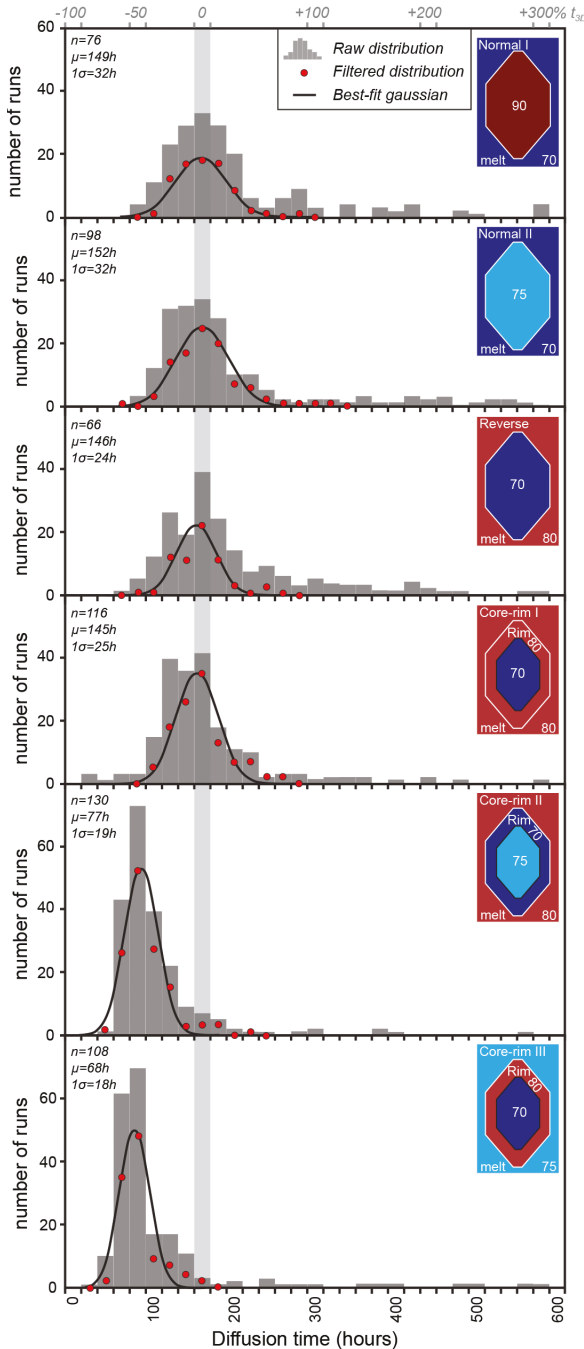


FIGURE 11. Accuracy and precision of timescales retrieved from 1D models. The time distributions in gray are the raw histograms with 200 profiles (cf. red curves in Fig. 9) while the red circles show the same distributions filtered for “unsuitable” olivines (see text for details). Black curves are best-fit Gaussians with accompanying mean and standard deviation values.

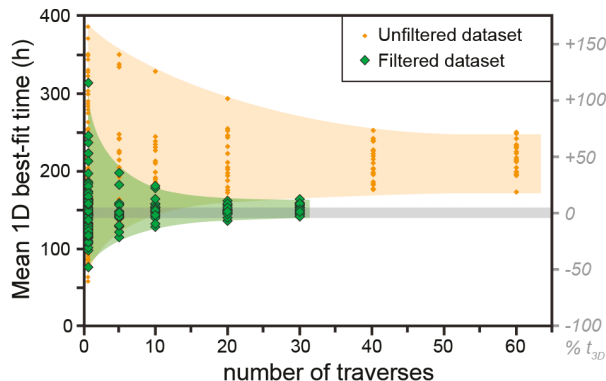


FIGURE 12. Number of concentration profiles necessary to obtain accurate diffusion timescales from a given olivine population. Except for the data corresponding to a single traverse (left-most points), each symbol represents the average of a set of 5, 10, 20, 30, 40, or 60 traverses. Both the unfiltered and filtered timescale data sets are shown.

typically ranges from ~30 to 70% of the total (Fig. 11). The “filtered” sections give few time overestimations and also show less prominent secondary modes or shoulders. Gaussian curves can be fitted to these distributions, and give mean values that are very close to the true 3D time for the three simple zoning styles (normal I and II and reverse) as well as the rim-core I zoning, (from 145 to 152 h, or an accuracy of 1–2% the total time, Fig. 11). For core-rim zonings II and III, as well as for longer duration (~1152 h) normal zoning II models (Supplementary Material¹), the mean value underestimates the true value by about half. This result is expected since the issues of underestimating timescales for these zonings stems from loss of rim plateau concentrations and not from poor selection of olivine sections. Irrespective of zoning style, the standard deviations or “precision” varies between 18–32 h, or typically ~15–25% the mean times. Therefore, providing the crystal sections are carefully selected, it can be estimated that 1D timescales will replicate the true diffusion times with a very high degree of accuracy (<5% from the true time) and reasonable precision (15–25% the calculated mean time).

How many sections/profiles are necessary to obtain accurate results?

The numerical models from this study also allow estimating the minimum number of concentration profiles required to establish the timescale of diffusion in a single olivine population accurately. The series of 200 one-dimensional models performed using the “reverse” zoning configuration (“raw data”) as well as the 66 models that adhered to the criteria above (“filtered data”) were used for this exercise. From the raw and filtered data, sets of 5, 10, 20, 40, and 60 timescales obtained by 1D models were sampled 20 times in a random fashion, and the mean time was computed for each subset. This random sampling provides a notion of variability, expressed by the mean of a given distribution of timescales as a function of the total number of traverses. For the raw data set, increasing the number of analytical profiles decreases the variability of obtained mean diffusion times, but only for a large number of profiles (40 profiles) (Fig. 12). In addition, the calculated means converge around a time t_{1D}^*

= 170–250 h, which is largely over the true diffusion time of 144 h. This result is somewhat expected considering the large number of time overestimates within the raw data, in addition to the non-normal nature of the timescale distribution (cf. Fig. 9b). In contrast, the filtered data yields timescales close to the true value when at least 20 profiles are used (Fig. 12). Thus, in addition to following the olivine section guidelines detailed above, it is recommended that for a given crystal population about 20 analytical profiles should be obtained to ensure timescale accuracy. Even though the numerical experiments were constructed to represent nature inasmuch as practically feasible, the crystal populations investigated all derived from one single-crystal size, and a homogeneously well-recorded diffusion event of 144 h. Therefore, more complex natural cases may warrant more than 20 transects.

ACKNOWLEDGMENTS

T.S. and J.H. are thankful for NSF EAR Grants 1321890 and 0948728, which funded this project. F.C. and D.K.’s work was funded by NRF-MoE Singapore “Magma Plumbing systems” Grant. Many ideas developed for this paper originated from the invaluable lectures, practicals, and discussions that took place during the 2012 Diffusion Workshop at the Ruhr-Universität Bochum, organized by Sumit Chakraborty, Ralf Dohmen, Thomas Müller, Sascha Borinski, Maren Kahl, Sabrina Schwinger, and Kathrin Faak. Bruce Watson is thanked for the sensible editorial handling, and two anonymous reviewers are thanked for the constructive comments that enhanced this contribution in many ways.

REFERENCES CITED

- Albarède, F., and Bottinga, Y. (1972) Kinetic disequilibrium in trace element partitioning between phenocrysts and host lava. *Geochimica et Cosmochimica Acta*, 36, 141–156.
- Bindeman, I.N., Sigmarsson, O., and Eiler, J. (2006) Time constraints on the origin of large volume basalts derived from O-isotope and trace element mineral zoning and U-series disequilibria in the Laki and Grimsvotn volcanic system. *Earth and Planetary Science Letters*, 245, 245–259.
- Bryan, W.B. (1972) Morphology of quench crystals in submarine basalts. *Journal of Geophysical Research*, 77, 5812–5819.
- Cardozo, N., and Allmendinger, R.W. (2013) Spherical projections with OSX Stereonet. *Computers and Geosciences*, 51, 193–205.
- Chakraborty, S. (1995) Diffusion in silicate melts. *Reviews in Mineralogy and Geochemistry*, 32, 411–504.
- (1997) Rates and mechanisms of Fe-Mg interdiffusion in olivine at 980–1300 °C. *Journal of Geophysical Research*, 102, 12317–12331.
- (2008) Diffusion in solid silicates: a tool to track timescales of processes comes of age. *Annual Reviews in Earth and Planetary Sciences*, 36, 153–190.
- (2010) Diffusion coefficients in olivine, wadsleyite and ringwoodite. *Reviews in Mineralogy and Geochemistry*, 72, 603–639.
- Cherniak, D.J. (2010) Cation diffusion in feldspars. *Reviews in Mineralogy and Geochemistry*, 72, 691–733.
- Coogan, L.A., Hain, A., Stahl, S., and Chakraborty, S. (2005) Experimental determination of the diffusion coefficient for calcium in olivine between 900 and 1500 °C. *Geochimica et Cosmochimica Acta*, 69, 3683–3694.
- Coombs, M.L., Eichelberger, J.C., and Rutherford, M.J. (2000) Magma storage and mixing conditions for the 1953–1974 eruptions of Southwest Trident volcano, Katmai National Park, Alaska. *Contributions to Mineralogy and Petrology*, 140, 99–118.
- Cooper, K.M., and Kent, A.J.R. (2014) Rapid remobilization of magmatic crystals kept in cold storage. *Nature*, 506, 480–483.
- Costa, F., and Chakraborty, S. (2004) Decadal time gaps between mafic intrusion and silicic eruption obtained from chemical zoning patterns in olivine. *Earth and Planetary Science Letters*, 227, 517–530.
- Costa, F., and Dungan, M. (2005) Short timescales of magmatic assimilation from diffusion modelling of multiple elements in olivine. *Geology*, 33, 837–840.
- Costa, F., Chakraborty, S., and Dohmen, R. (2003) Diffusion coupling between trace and major elements and a model for calculation of magma residence times using plagioclase. *Geochimica et Cosmochimica Acta*, 67, 2189–2200.
- Costa, F., Dohmen, R., and Chakraborty, S. (2008) Timescales of magmatic processes from modeling the zoning patterns of crystals. *Reviews in Mineralogy and Geochemistry*, 69, 545–594.
- Costa, F., Coogan, L.A., and Chakraborty, S. (2010) The timescales of magma mixing and mingling involving primitive melts and melt-mush interaction at mid-ocean ridges. *Contributions to Mineralogy and Petrology*, 159, 173–194.

Crank, J. (1975) *The Mathematics of Diffusion*, 2nd edition, 414 p. Oxford Science Publication, Oxford.

Demouchy, S., Jacobsen, S.D., Gaillard, F., and Stern, C.R. (2006) Rapid magma ascent recorded by water diffusion profiles in mantle olivine. *Geology*, 34, 429–432.

Dohmen, R., and Chakraborty, S. (2007) Fe-Mg diffusion in olivine II: Point defect chemistry, change of diffusion mechanisms and a model for calculation of diffusion coefficients in natural olivine. *Physics and Chemistry of Minerals*, 34, 409–430.

Druitt, T.H., Costa, F., Deloule, E., Dungan, M., and Scailet, B. (2012) Decadal to monthly timescales of magma transfer and reservoir growth at a caldera volcano. *Nature*, 482, 77–80.

Faure, F., Trolliard, G., Nicollet, C., and Montel, J.M. (2003) A developmental model of olivine morphology as a function of the cooling rate and the degree of undercooling. *Contributions to Mineralogy and Petrology*, 145, 251–263.

Faure, F., Arndt, N., and Libourel, G. (2006) Formation of spinifex texture in komatiites: An experimental study. *Journal of Petrology*, 47, 1591–1610.

Faure, F., Schiano, P., Trolliard, G., Nicollet, C., and Soulestin, B. (2007) Textural evolution of polyhedral olivine experiencing rapid cooling rates. *Contributions to Mineralogy and Petrology*, 153, 405–416.

Ganguly, J. (2002) Diffusion kinetics in minerals: Principles and applications to tectono-metamorphic processes. *European Mineralogical Union*, 4, 271–309.

Ganguly, J., Dasgupta, S., Cheng, W., and Neogi, S. (2000) Exhumation history of a section of the sikkim Himalayas, India: records in the metamorphic mineral equilibria and compositional zoning of garnet. *Earth and Planetary Science Letters*, 183, 471–486.

Girona, T., and Costa, F. (2013) DIPRA: A user-friendly program to model multi-element diffusion in olivine with applications to timescales of magmatic processes. *Geochemistry, Geophysics, Geosystems*, 14, 422–431.

Hammer, J.E., Sharp, T.G., and Wessel, P. (2010) Heterogeneous nucleation and epitaxial crystal growth of magmatic minerals. *Geology*, 38, 367–370.

Ishibashi, H., Arakawa, M., Ohi, S., Yamamoto, J., Miyake, A., and Kagi, H. (2008) Relationship between Raman spectral pattern and crystallographic orientation of a rock-forming mineral: A case study of $\text{Fo}_{89}\text{Fa}_{11}$ olivine. *Journal of Raman Spectroscopy*, 39, 1653–1659.

Ito, M., and Ganguly, J. (2006) Diffusion kinetics of Cr in olivine and ^{53}Mn - ^{53}Cr thermochronology of early solar system objects. *Geochimica et Cosmochimica Acta*, 70, 799–809.

Kahl, M., Chakraborty, S., Costa, F., and Pompilio, M. (2011) Dynamic plumbing system beneath volcanoes revealed by kinetic modeling and the connection to monitoring data: An example from Mt. Etna. *Earth and Planetary Science Letters*, 308, 11–22.

Kahl, M., Chakraborty, S., Costa, F., Pompilio, M., Liuzzo, M., and Viccaro, M. (2013) Compositionally zoned crystals and real-time degassing data reveal changes in magma transfer dynamics during the 2006 summit eruptive episodes of Mt. Etna. *Bulletin of Volcanology*, 75, 1–14.

Longpre, M.-A., Klugel, A., Diehl, A., and Stix, J. (2014) Mixing in mantle magma reservoirs prior to and during the 2011–2012 eruption at El Hierro, Canary Islands. *Geology*, 42, 315–318.

Marti, J., Castro, A., Rodriguez, C., Costa, F., Carrasquilla, S., Pedreira, R., and Bolos, X. (2013) Correlation of magma evolution and geophysical monitoring during the 2011–2012 El Hierro (Canary Islands) submarine eruption. *Journal of Petrology*, 54, 1349–1373.

Milman-Barris, M.S., Beckett, J.R., Michael, M.B., Hofmann, A.E., Morgan, Z., Crowley, M.R., Vielzeuf, D., and Stolper, E. (2008) Zoning of phosphorus in igneous olivine. *Contributions to Mineralogy and Petrology*, 155, 739–765.

Morgan, D.J., Blake, S., Rogers, N.W., DeVivo, B., Rolandi, G., Macdonald, R., and Hawkesworth, J. (2004) Timescales of crystal residence and magma chamber volume from modeling of diffusion profiles in phenocrysts: Vesuvius 1944. *Earth and Planetary Science Letters*, 222, 933–946.

Morgan, D.J., Blake, S., Rogers, N.W., DeVivo, B., Rolandi, G., and Davidson, J. (2006) Magma recharge at Vesuvius in the century prior to the eruption AD 79. *Geology*, 34, 845–848.

Nakamura, M. (1995) Residence time and crystallization history of nickeliferous olivine phenocrysts from the northern Yatsugatake volcanoes, Central Japan: Application of a growth and diffusion model in the system Mg-Fe-Ni. *Journal of Volcanology and Geothermal Research*, 66, 81–100.

Onsager, L. (1945) Theories and problems of liquid diffusion. *Annals of the New York Academy of Sciences*, 46, 241–265.

Pan, Y., and Batiza, R. (2002) Mid-ocean ridge magma chamber processes: Constraints from olivine zonation in lavas from the East Pacific Rise at $9^{\circ}30'\text{N}$ and $10^{\circ}30'\text{N}$. *Journal of Geophysical Research*, 107, 2022.

Pankhurst, M.J., Dobson, K.J., Morgan, D.J., Loughlin, S.C., Thordarson, T., Lee, P.D., and Courtois, L. (2014) Monitoring the magmas fuelling volcanic eruptions in near-real-time using X-ray micro-computed tomography. *Journal of Petrology*, 55, 671–684.

Pearce, T.H. (1984) The analysis of zoning in magmatic crystals with emphasis on olivine. *Contributions to Mineralogy and Petrology*, 86, 149–154.

Petry, C., Chakraborty, S., and Palme, H. (2004) Experimental determination of Ni diffusion coefficients in olivine and their dependence on temperature, composition, oxygen fugacity, and crystallographic orientation. *Geochimica et Cosmochimica Acta*, 68, 4179–4188.

Pilbeam, L.H., Nielsen, T.F.D., and Waught, T.E. (2013) Digestion fractional crystallization (DFC): An important process in the genesis of kimberlites. Evidence from olivine in the Majuagaa kimberlite, southernwest Greenland. *Journal of Petrology*, 54, 1399–1425.

Prior, D.J., Boyle, A.P., Brenker, F., Cheadle, M.C., Day, A., Lopez, G., Peruzzo, L., Potts, G.J., Reddy, S.M., Spiess, R., Timms, N.E., Trimby, P.W., Wheeler, J., and Zetterström, L. (1999) The application of electron backscatter diffraction and orientation contrast imaging in the SEM to textual problems in rocks. *American Mineralogist*, 84, 1741–1759.

Ruprecht, P., and Cooper, K.M. (2012) Integrating uranium-series and elemental diffusion geochronometers in mixed magmas from Volcan Quizapu, Central Chile. *Journal of Petrology*, 53, 841–871.

Ruprecht, P., and Plank, T. (2013) Feeding andesitic eruptions with a high-speed connection from the mantle. *Nature*, 500, 68–72.

Saltikov, S.A. (1967) The determination of the size distribution of particles in an opaque material from a measurement of the size distribution of their sections. In H. Elias, Ed., *Stereology*, pp. 163–173. Springer-Verlag, New York.

Saunders, K., Blundy, J., Dohmen, R., and Cashman, K. (2012) Linking petrology and seismology at an active volcano. *Science*, 336, 1023–1027.

Shea, T., and Hammer, J.E. (2013) Kinetics of cooling- and decompression-induced crystallization in hydrous mafic-intermediate magmas. *Journal of Volcanology and Geothermal Research*, 260, 127–145.

Sio, C.K., Dauphas, N., Teng, F.-Z., Chaussidon, M., Helz, R.T., and Roskosz, M. (2013) Discerning crystal growth from diffusion profiles in zoned olivine by in-situ Mg-Fe isotopic analyses. *Geochimica et Cosmochimica Acta*, 123, 302–321.

Spandler, C., and O'Neill, H.S.C. (2010) Diffusion and partition coefficients of minor and trace elements in San Carlos olivine at 1300°C with some geochemical implications. *Contributions to Mineralogy and Petrology*, 159, 791–818.

Wallace, G.S., and Bergantz, G.W. (2004) Constraints on mingling of crystal populations from off-center zoning profiles: A statistical approach. *American Mineralogist*, 89, 64–73.

Watson, E.B. (1994) Diffusion in volatile-bearing magmas. *Reviews in Mineralogy*, 30, 371–411.

Watson, E.B., and Baxter, E.F. (2007) Diffusion in solid-Earth systems. *Earth and Planetary Science Letters*, 253, 307–327.

Watson, E.B., Wanzer, K.H., and Farley, K.A. (2010) Anisotropic diffusion in a finite cylinder, with geochemical applications. *Geochimica et Cosmochimica Acta*, 74, 614–633.

Welsch, B., Faure, F., Bachèlery, P., and Famin, V. (2009) Microcrysts record transient convection at Piton de la Fournaise volcano (La Reunion hotspot). *Journal of Petrology*, 50, 2287–2305.

Welsch, B., Faure, F., Famin, V., Baronnet, A., and Bachèlery, P. (2013) Dendritic crystallization: a single process for all the textures of olivine in basalts? *Journal of Petrology*, 54, 539–574.

Zellmer, G.F., Blake, S., Vance, D., Hawkesworth, C., and Turner, S. (1999) Plagioclase residence times at two island arc volcanoes (Kameni Islands, Santorini, and Soufrière, St. Vincent) determined by Sr diffusion systematics. *Contributions to Mineralogy Petrology*, 136, 345–357.

Zhang, Y. (2010) Diffusion in minerals and melts: Theoretical background. *Reviews in Mineralogy and Geochemistry*, 72, 5–59.

MANUSCRIPT RECEIVED AUGUST 13, 2014

MANUSCRIPT ACCEPTED APRIL 2, 2015

MANUSCRIPT HANDLED BY BRUCE WATSON